Dynamic Stress Analysis of Smooth and Notched Fiber Composite Flexural Specimens

P. L. N. Murthy and C. C. Chamis
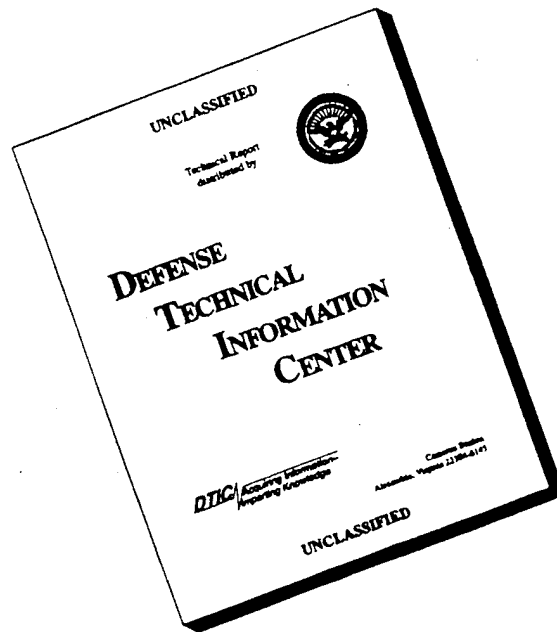*Lewis Research Center*
Cleveland, Ohio

DTIC QUALITY INSPECTED 4

NASA

DEPARTMENT OF DEFENSE
PLASTICS TECHNICAL EVALUATION CENTER
ARRADCOM, DOVER, N. J.   07801

19960226 007

DISCLAIMER NOTICE

THIS DOCUMENT IS BEST QUALITY AVAILABLE. THE COPY FURNISHED TO DTIC CONTAINED A SIGNIFICANT NUMBER OF PAGES WHICH DO NOT REPRODUCE LEGIBLY.

TABLE OF CONTENTS

DYNAMIC STRESS ANALYSIS OF SMOOTH AND NOTCHED FIBER

COMPOSITE FLEXURAL SPECIMENS

P. L. N. Murthy and C. C. Chamis
National Aeronautics and Space Administration
Lewis Research Center
Cleveland, Ohio 44135

SUMMARY

A detailed analysis of the dynamic stress field in smooth and notched fiber composite (Charpy-type) specimens is reported in this paper. The analysis is performed with the aid of the direct transient response analysis solution sequence of MSC/NASTRAN. Three unidirectional composites were chosen for the study. They are S-Glass/Epoxy, Kevlar/Epoxy and T-300/Epoxy composite systems. The specimens are subjected to an impact load which is modeled as a triangular impulse with a maximum of 2000 lb and a duration of 1 ms. The results are compared with those of static analysis of the specimens subjected to a peak load of 2000 lb. For the geometry and type of materials studied, the static analysis results gave close conservative estimates for the dynamic stresses. Another interesting inference from the study is that the impact induced effects are felt by S-Glass/Epoxy specimens sooner than Kevlar/Epoxy or T-300/Epoxy specimens.

INTRODUCTION

Smooth and notched flexural specimen testing continues to be popular in the composites community for characterizing and/or qualifying fiber composites. Reasons for the popularity are: (1) simplicity, (2) adaptability to adverse environments, (3) availability of simple equations for data reduction, and (4) availability of written ASTM standard testing procedures. In addition to these reasons, flexural specimen testing forces the material to respond like a structure by simultaneously subjecting it to tensile, compressive and shear stresses. Furthermore, the notched flexural specimen (Charpy impact test specimen) testing enables easy determination of fracture toughness and impact resistance.

Fracture in general (be it static, quasi-static or dynamic) is a dynamic event and, as such, is a very complex process. Fracture progression in a flexural specimen is controlled by the local dynamic stress field which is also complex. The local dynamic stress field is characterized by the stress waves which are normal, shear, flexural and surface waves. Each of the dynamic stresses can initiate failure (or a defect) at a point and/or propagate this defect to fracture. For a complete understanding of these phenomena a detailed description of the local dynamic stress field is a prerequisite. This requires the use of a complex transient analysis involving direct time integration as opposed to the standard modal synthesis methods such as those available in some general purpose finite element structural analysis codes. Solution 27 (direct transient response) of MSC/NASTRAN is one of the available tools for such analyses. The objective of the present paper is to report a detailed analysis of the dynamic stress field in smooth and notched Charpy specimens.

Although the notched Charpy test specimen has been used for years in testing metals and recently in testing composites, no analysis has been performed to determine the detailed dynamic stress state variation in the notch vicinity. In general, the physical problem of the notched Charpy test specimen is dynamic and nonlinear; solution of this problem is difficult. However, a good first order approximation may be obtained by assuming linear behavior and a quasi-static load. Reference 1 reports such an analysis which uses the static solution sequence of COSMIC NASTRAN. The main conclusions of reference 1 are: 1) the stress state is biaxial, and 2) the Charpy test specimen is not suitable for assessing the impact resistance of nonmetallic fiber composites directly. In the present work the effort is directed towards understanding the stress wave propagation and the attendant dynamic stress field in fiber composite smooth and notched flexural specimens.

ANALYSIS

In this section, the specimen geometry, the finite element idealization, the finite element analysis method, and the composite systems analyzed are described.

Specimen Geometry

The geometry of the Charpy test specimen (ASTM STD E23-7) is shown in figure 1. As can be seen in this figure, the overall length of the specimen is 2.164 in. and the length between supports is 1.574 in. The specimen width is 0.394 in. The specimen unnotched depth is 0.394 in. and the depth at the notch is 0.315 in. The notch is 0.079 in. deep and has a 45° opening.

Finite Element Idealization

Two finite element idealizations of Charpy test specimens -- one without a notch (smooth specimen) and one with a notch were selected for the present study. The details of the meshes are shown in figures 2 and 3. The material properties are assumed to be uniform, orthotropic, and obey a linear stress-strain law throughout the analysis. In addition, the specimen is assumed to be in a state of plane stress. The plane stress assumption is also justified from the physics of the problem. The width restraints at the notch-tip are negligible because of the very low value of the respective Poisson's ratio. For the present analysis, the plane stress assumption implies that the stresses are permitted to vary along the specimen length and through the thickness but not across the width. This reduces the stresses to be calculated to three, two normal and one shear.

With these assumptions, plane stress finite elements can be used to model the Charpy test specimen. For the smooth specimen all the elements are quadrilateral. The notched specimen is modeled with both triangular elements and quadrilateral elements. The triangular elements are used as transition elements in the areas around the the supports, the load application point and the notch. These are the regions where maximum stress concentrations are expected to occur and therefore are provided with a finer mesh. The boundary conditions prescribed are such that the node at the left support is constrained from x, y and z displacements, and the node at the right support is constrained from y

and z displacements. In addition, for the notched specimen, three nodes clos-
est to the right support are constrained from displacement in the y direction.
The specimens are subjected to an impulse loading. The form of impact is a
triangular function with peak load of 2000 lb occuring at 500 μs of a total
contact time of 1000 μs.

The statistics of the finite element representation for the smooth and
notched specimens are as follows:

1) Smooth Specimens.
    Number of nodes or grid points   1147
    Number of displacement degrees of freedom (DOF) (2 degrees
        of freedom per node)   2294
    Number of quadrilateral plate elements (CQUAD4)   1080
    DOF eliminated using the boundary conditions (2 from u = 0
        and v = 0 at the left support and 1 from v=0 at the
        right support)   3
    Number of free DOF (2294 - 3)   2291

2) Notched Specimens.
    Number of nodes or grid points   656
    Number of displacement degrees of freedom (DOF)   1312
    Number of quadrilateral plate elements (CQUAD4)   544
    Number of triangular plate elements (CTRIA3)   82
    Total number of elements (544 + 82)   626
    DOF eliminated using the boundary conditions (2 from u = 0
        and v = 0 at the left support and 3 from v = 0 for three
        nodes at the right support)   5
    Number of free DOF (1312 - 5)   1307

Finite Element Analysis Method

The MSC/NASTRAN general purpose structural analysis finite element com-
puter program is used for the finite element analysis. The specific elements
used are identified as CTRIA3 and CQUAD4. They are isoparametric constant
strain elements. NASTRAN obtains the solution using a displacement formulation
via rigid format solution sequence No. 27. This solution sequence employs a
direct time integration scheme to obtain the transient response of a structure.

The solution sequence No. 27 of MSC/NASTRAN uses the integration algorithm
based upon the Newmark Beta method (ref. 2). It provides stable results for
the widest possible spectrum of practical problems without sacrificing either
accuracy or efficiency. For complete details of the MSC/NASTRAN analysis
(ref. 3) should be consulted. A brief description is given in the following
paragraphs.

The differential equations of a linear structural problem may be written
in the general matrix form

$$[p^2 M + pB + K] \{u\} = \{F\} \tag{1}$$

where $p = d/dt$. M and K are the mass and stiffness matrices, B is asso-
ciated with the damping matrix, u is the vector of displacements and F is
the load vector. The numerical integration is achieved by replacing p^2 and
p by finite difference operators and then using explicit integration. The

3

outputs of the transient analysis module include velocities, and accelerations as well as displacements. The output can be requested at even multiples of the integration time step. This feature affords some economy in output data preparation in cases where small time step is needed for greater accuracy.

Composite Systems Analyzed

Flexural (Charpy-type) test specimens made from three typical composite systems are analyzed. They are: T-300/Epoxy, Kevlar/Epoxy, and S-Glass/Epoxy composites. The specimens are all unidirectional composites with the fibers parallel to the length (x-axis, fig. 1) of the specimen.

The plane stress-strain relationship (stiffness) coefficients required to input to NASTRAN are summarized in table I. These properties are obtained by using the resident data-bank in the composite mechanics computer code ICAN (ref. 4). The relationships between the NASTRAN stiffness coefficients (G's), and the usual engineering constants are:

$$G_{11} = E_{\ell 11}/(1 - \nu_{\ell 12}\,\nu_{\ell 21}) \tag{2}$$

$$G_{12} = \nu_{\ell 21}\,G_{11} = \nu_{\ell 12}\,G_{22} = G_{21} \tag{3}$$

$$G_{22} = E_{\ell 22}/(1 - \nu_{\ell 12}\,\nu_{\ell 21}) \tag{4}$$

$$G_{33} = G_{\ell 12} \tag{5}$$

$$G_{13} = G_{23} = G_{31} = G_{32} = 0 \tag{6}$$

The notation in equations (2) to (5) is as follows: $E_{\ell 11}$ denotes the longitudinal modulus, $E_{\ell 22}$ the transverse modulus, $G_{\ell 12}$ the shear modulus, $\nu_{\ell 12}$ the major Poisson's and $\nu_{\ell 21}$ the minor Poisson's ratios. For an elastic material the two Poisson's ratios are related by the well known relation

$$\nu_{\ell 21} = \nu_{\ell 12}\,E_{\ell 22}/E_{\ell 11} \tag{7}$$

RESULTS AND DISCUSSION

Load conditions

Two types of load conditions are used in obtaining the results. The first is a static loading where a force of 2000 lb is applied at the center of the specimen on the top surface. The second is an impulse loading. This is modeled as a triangular pulse with a peak value of 2000 lb in the middle. The pulse is modeled to last for 1000 μs. The transient response is, however, obtained for three contact time periods (i.e., 3 ms). A separate normal modes analysis is used to determine the first five natural frequencies.

Natural Frequencies and Normal Modes

The NASTRAN normal modes analysis module (Solution 3) is utilized to determine the first five natural frequencies and the associated mode shapes for

the Charpy test specimens. They are shown in figure 4. The results are shown
in table II for S-Glass/Epoxy specimens. The frequencies are used to determine
the time periods which aid in determining the integration time step for the
transient analysis. A time step of 5 μs is chosen for the transient analysis
based upon the time periods shown in table II.

Displacement and Stress Wave Propagation

The bulk wave and shear wave velocities are normally much higher compared
to the flexural wave velocities. In order to capture the characteristics of
propagation of these waves a much smaller time step of integration (0.1 μs) is
chosen. The output of displacements and stress contours at various time inter-
vals are saved and displayed graphically in figures 5 to 10. Figures 5 to 7
depict the dynamic displacement propagation in S-Glass/Epoxy, Kevlar/Epoxy and
T-300/Epoxy specimens. Two bulk wave velocity parameters and one shear wave
velocity parameter are defined below to aid the following discussion of the
displacement wave propagation results:

$$C_{B11} = G_{11}/\rho \tag{8}$$

$$C_{B22} = G_{22}/\rho \tag{9}$$

$$C_{S12} = G_{12}/\rho \tag{10}$$

where ρ is the mass density of the material.

The computed values of C_{B11}, C_{B22}, and C_{S12} are shown in table III for
the three composite systems under study. The velocities are expressed in
in./μs. The trend indicated by C_{B22} for the three materials (the transverse
shock wave travels fastest in S-Glass/Epoxy and slowest in Kevlar/Epoxy) is
seen clearly in figures 5 to 7 specifically the frames after 3 and 5 μs. A
rough estimate of the normal wave velocity can be obtained by counting the
number of elements that appear to be affected by the impact from the figures 5
to 7. The normal wave velocity estimates from the 1 and 3 sec frames are shown
below:

Composite system	Number of elements		Velocity		Average
	1 μsec	3 μsec	1 μsec	3 μsec	
S-Glass/Epoxy	10	25	0.1313	0.1094	0.1204
T-300/Epoxy	7	16	.0788	.0700	.0744
Kevlar/Epoxy	5	12	.0657	.0520	.0589

These values are in close agreement with the theoretical values shown in
table III under C_{B22}. The same trend is also seen for the 3 and 5 μ sec
frames. It can be concluded that the initial shock travels with the bulk wave
velocity C_{B22} along the direction of impact.

Once the normal shock reaches the bottom of the beam, the wavefront ap-
pears to be moving in the longitudinal direction forming a flexural wave. The
velocities of the waves traveling in the longitudinal direction can also be
determined approximately with the same technique mentioned earlier. The fol-
lowing are the details for the frame after 13 μs:

Composite system	Number of elements	Velocity
S-Glass/Epoxy	11	0.0510 in/μsec
T-300/Epoxy	9	.0416 in/μsec
Kevlar/Epoxy	7	.0320 in/μsec

The above velocities appear to have the same trend as depicted by the wave velocity parameter C_{S12} shown in table III. However, the waves along the longitudinal direction appear to move significantly slower than that indicated by C_{S12}. This is probably due to the coupling between the flexural wave and the shear wave. The flexural wave velocity is significantly slower than the shear wave velocity. For example, the smooth S-Glass/Epoxy specimen under study has a flexural wave velocity given by

$$C_F = 2\ell f = 0.0137 \text{ in/μsec}$$

where ℓ is the length between the supports, f is the first fundamental frequency. (It is assumed that the wave number is 1 and the beam deflects into a half wave.)

The transient stress response after one percent (10 μs) of the contact time are shown in figures 8 to 10 in the form of stress contours. All stresses are localized at this early time. The longitudinal stress (σ_{11}) in the Kevlar/Epoxy and T-300/Epoxy composites is of about the same magnitude while that in the S-Glass/Epoxy is about half as much. The normal stress (σ_{22}) and shear stress (σ_{12}) are of about the same magnitude for all three composite systems. It appears from these stress results that, under the same impact conditions, the stress in the Kevlar/Epoxy and the T-300/Epoxy will reach fiber fracture stress magnitudes considerably earlier (about half the time) than in the S-Glass/Epoxy composite. Two implications follow relative to the same stress magnitude: (1) the S-Glass/Epoxy composite will sustain greater impact load prior to fracture than the T-300/Epoxy, and (2) the rapid compressive stress built up will cause longitudinal compression failure accompanied by substantial bending deflection in the Kevlar/Epoxy composite thus increasing the impact required to induce fracture.

Transient Response of Smooth Specimens

The displacements, velocities, accelerations and stresses are obtained for a total contact time of 1000 μs for S-Glass/Epoxy smooth specimens. In these computations a time step of 5 μs is used. The output is saved for every two time steps. Two points A and B as shown in figures 2 and 3 are selected for study. A is the load point and B is the opposite point at the bottom for smooth and at the notch-tip for notched specimens.

The transient response results appear in figures 11 to 16. Figures 11 to 13 show the longitudinal (axial) and the transverse (bending/flexural) components of displacement, velocity and acceleration of point A plotted against time. The corresponding results for point B are not shown as they are similar to point A response both qualitatively and quantitatively. It can be concluded from these figures that the response is primarily in the first flexural mode. For example (from fig. 11) the number of cycles in 1 ms is counted as a little

over 6. From table II the first fundamental time period is 161.3 µs which implies that 6.2 (1000/161.3) cycles of response in first mode can be expected.

The stress response results are shown graphically in figures 14 to 16. Each figure contains the stress response of elements near points A and B. The longitudinal stress behavior appear to be primarily the first flexural mode response. However, the magnitude of stress near point A is about one and a half times greater than the magnitude of stress near point B. This is to be expected because of stress concentration near the load point A. The transverse normal (σ_{22}) and the shear (σ_{12}) stress increase linearly to a peak when the load takes the maximum value of 2000 lb and then decrease linearly to a zero. The corresponding stresses for the element near point B are insignificant and therefore can not be shown distinctly when drawn to the same scale.

The response after the load removal is not shown in the above figures. The computations, however, are conducted for three contact time periods. It is found that, for all practical purposes, the specimen remains static. A typical response curve is shown in figure 17 for point A.

Static and Dynamic Stress Contours

Smooth specimen. - The static stress contours under a load of 2000 lb and the dynamic stress contours at the peak load of 2000 lb are shown in figures 18 to 20. They appear to be identical. The peak values for the dynamic load case, however, are slightly lower than those for the static case. While the maxima for the longitudinal stress (σ_{11}) occur at the center of top and the bottom, the transverse normal stress and the transverse shear stress have the maxima almost adjacent to each other near the load application point. The transverse shear stress and the axial stress distribution is seen to approach the classical Euler-Bernoulli theory predictions away from the load application point. Steep stress gradients are observed near the load application point.

Notched specimen. - The results for notched S-Glass/Epoxy specimen are shown in figures 21 to 23. The static and dynamic stress contours at the peak load show similar trend as observed in the case of smooth specimens. Figure 24 shows the stress intensity near notch-tip in relation to the far field stresses. This distance from the notch-tip is measured along the longitudinal direction towards the left support. It is seen that all the three stresses attain very high peaks, indicating severe local stress intensities near the notch-tip. As the stress allowables for σ_{22} and σ_{12} are generally an order of magnitude lower than that for σ_{11}, one can expect a matrix initiated failure followed by fiber fractures at this location.

GENERAL DISCUSSION

The response analysis of smooth and notched Charpy-type flexural specimens subjected to a triangular impulsive load provides insight into the nature of stress wave propagation, failure mechanisms and the relation between the static and dynamic responses. The contact time of the impact load is approximately 6 time periods of the first flexural mode. The bulk wave velocities C_{B11} and C_{B22}, and the shear wave velocity C_{S12} are very high compared to the flexural wave velocity for the materials and the geometry under study. Hence, the response is observed at early times of the impact event (of the order of a microsecond). It shows that the initial waves travel with a bulk wave velocity

7

c_{B22} till they reach the bottom surface of the specimen. The waves then appear to travel longitudinally towards the supports. The approximate calculations based upon the deformations at various times indicated that the wave velocity is significantly lower than the shear wave velocity c_{S12} but much higher than the flexural wave velocity. The wavefront appears to induce a flexural wave as it progresses towards the supports.

At longer times, the response is primarily in the first flexural mode. A comparison with the static response indicates that little or no difference exists in the magnitude for stresses at the peak load. The static predictions, however, are on the conservative side.

The response of notched fiber composite specimens show severe stress intensities near the notch region indicating local failures in shear and transverse tension initially followed by fiber fractures since the longitudinal stresses approach fracture stress magnitudes.

The response after the load removal reduces to mere noise; the structure remains practically static.

SUMMARY OF RESULTS

The results of the study on static, dynamic and transient response of smooth and notched, fiber composite, Charpy specimens are listed below:

(1)   The wave propagation velocities can be estimated from the early time displacement propagation response; the estimates are in fair agreement with the theoretical predictions.

(2)   The first five flexural mode shapes and frequencies show coupling effects from the thickness stretch and the transverse shear type modes; the frequencies are not integer multiples of the fundamental frequency.

(3)   The dynamic and static peak load stress contours are almost identical. The static peak load stress magnitudes are slightly higher. Stress predictions based upon a quasi-static approach lead to conservative estimates.

(4)   The transient displacement and velocity response appear to be primarily in the first flexural mode. The acceleration response shows contributions from higher modes.

(5)   The structure responds for the load duration time period only. The steady state response after the load removal appears to be negligible.

(6)   The transverse normal and shear stresses vary linearly with time and follow the load path.

(7)   The notch-tip region develops severe stress concentrations and any of the three stresses could cause or initiate a failure.

(8)   Based upon the transient stress response, it appears that the failures in Charpy specimens are initiated at the notch-tip by the shear stresses and the transverse tensile stresses followed by fiber fractures. However, the

failures in smooth specimens are probably initiated by a combined stress state near the load application point followed by local interply delaminations.

REFERENCES

1. Chamis, C. C., "Failure Mechanics of Fiber Composite Notched Charpy Specimens," NASA TM X-73462, National Aeronautics and Space Administration, Lewis Research Center, Cleveland, OH, Sept. 1976.
2. Newmark, N. M., _American Society of Civil Engineers, Journal of the Engineering Mechanics Division_, EM-3, July 1959, pp. 67-94.
3. MacNeal, R. H., "The NASTRAN Theoretical Manual, (Level 15.5)," MacNeal-Schwendler Corp., Los Angeles, CA, Dec. 1972.
4. Murthy, P. L. N. and Chamis, C. C., "ICAN: Integrated Composite Analyzer: Users and Programmers Manuals, NASA TP; No. to be assigned, National Aeronautics and Space Administration, Lewis Research Center, Cleveland, OH, 1984.

TABLE I. - NASTRAN PLANE STRESS - STRAIN RELATIONSHIPS

Composite system	Mass density $(\times 10^4)$ $(lb.sec^2/in^4)$	Stress-strain coefficient			Orthotropy Ratios		
		G_{11}	$G_{12} = G_{21}$	G_{22} $(\times 10^6 \text{ psi})$	G_{33}	G_{11}/G_{22}	G_{11}/G_{33}
S-Glass /Epoxy	1.813	8.7900	1.1700	3.2600	1.2700	2.70	6.92
Kevlar /Epoxy	1.249	12.385	.20082	.57377	.31635	21.59	39.15
T-300 /Epoxy	1.405	17.896	.30275	1.1318	.50871	15.81	35.18

TABLE II. - NATURAL FREQUENCIES AND TIME
PERIODS FOR S-GLASS/EPOXY SMOOTH AND
NOTCHED SPECIMENS

Specimen type	Mode number	Frequency (cycles/sec)	Time period (µs)
Smooth	1	6200.57	161.3
	2	11659.54	85.8
	3	19993.02	50.2
	4	31062.8	32.2
	5	43913.02	22.8
Notched	1	9030.16	110.7
	2	14631.33	68.3
	3	24596.56	40.7
	4	27775.86	36.0
	5	36685.27	27.3

TABLE III. – WAVE VELOCITY PARAMETERS
FOR THE SELECTED COMPOSITE SYSTEMS

Parameter Material	C_{B11}	C_{B22}	C_{S12}
S-Glass/Epoxy	0.2201	0.1341	0.0837
Kevlar/Epoxy	.3149	.0679	.0503
T-300/Epoxy	.3569	.0898	.0602
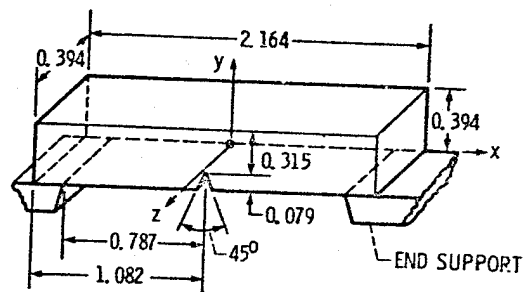
Figure 1. - Geometry of ASTM Charpy test specimen.
(All dimensions in inches.)
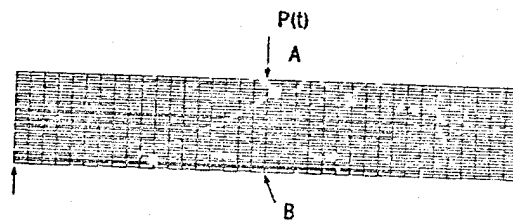
Figure 2. - Finite element idealization of smooth specimen.
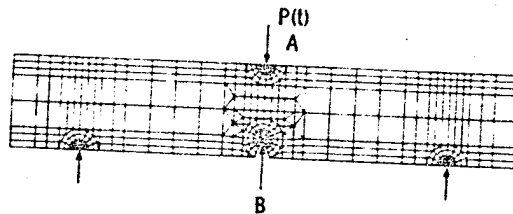
Figure 3. - Finite element idealization of notched Charpy specimen.

1. f = 6200. 67 Hz.

1. f = 9030. 157 Hz.

2. f = 11659. 54 Hz.

2. f = 14631. 33 Hz.

3. f = 19993. 02 Hz.

3. f = 24596. 56 Hz.

4. f = 31062. 80 Hz.

4. f = 27775. 86 Hz

5. f = 43913. 02 Hz.

5. f = 36685. 27 Hz.
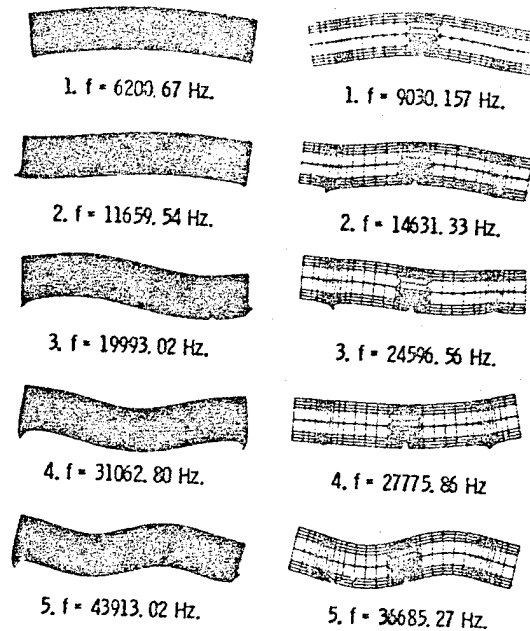
Figure 4. - Natural frequencies and mode shapes for S-glass/epoxy smooth and notched flexural specimens.

1 μsec

10 μsec

3 μsec

13 μsec

5 μsec

15 μsec

6 μsec

18 μsec

9 μsec

20 μsec

Figure 5. - Dynamic displacement propagation in S-glass/
epoxy composite flexural specimen. (Triangular impulse:
2000 lb maximum 1000 μsec duration.)

1 μsec

10 μsec

3 μsec

13 μsec

5 μsec

15 μsec

6 μsec

18 μsec

9 μsec

20 μsec
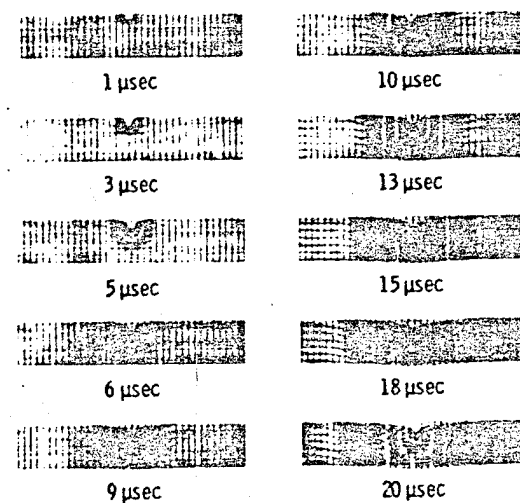
Figure 6. - Dynamic displacement propagation in Kevlar/
epoxy composite flexural specimen. (Triangular impulse:
2000 lb maximum 1000 μsec duration.)
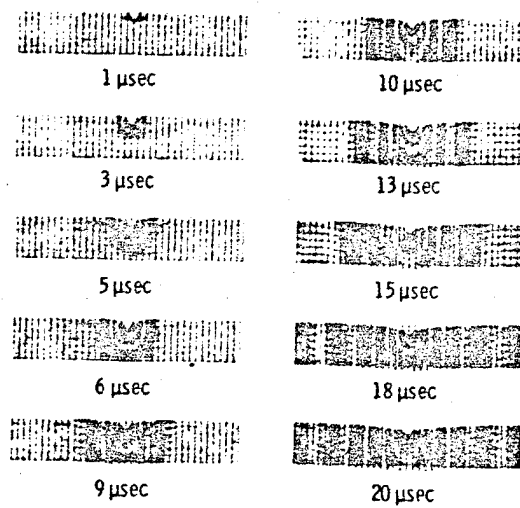
Figure 7. – Dynamic displacement propagation in T-300/
epoxy composite flexural specimen. (Triangular impulse:
2000 lb maximum 1000 μsec duration.)

SYMBOL VALUES, psi

1	-1.326899E+03
2	-1.143674E+03
3	-9.584489E+02
4	-7.732237E+02
5	-5.879985E+02
6	-4.027733E+02
7	-2.175482E+02
8	-3.232298E+01
9	1.529022E+02
10	3.381274E+02

SYMBOL VALUES, psi

1	-2.362948E+03
2	-2.065930E+03
3	-1.768912E+03
4	-1.471895E+03
5	-1.174877E+03
6	-8.778589E+02
7	-5.308411E+02
8	-2.838233E+02
9	1.319453E+01
10	3.102123E+02
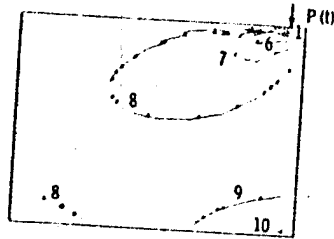
(a) σ_{11} Contours.

(a) σ_{11} Contours.

1	-1.052444E+03
2	-9.068754E+02
3	-7.613066E+02
4	-6.157379E+02
5	-4.701691E+02
6	3.246003E+02
7	1.790316E+02
8	3.346283E+01
9	1.121059E+02
10	2.576747E+02
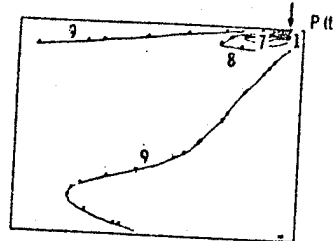
1	-1.913533E+03
2	-8.775216E+02
3	-7.415100E+02
4	-6.054954E+02
5	-4.694862E+02
6	-3.334752E+02
7	-1.974635E+02
8	-6.145193E+01
9	7.455969E+01
10	2.105713E+02

(b) σ_{22} Contours.

(b) σ_{22} Contours.

1	-5.760680E+02
2	-4.970201E+02
3	-4.120802E+02
4	-3.689114E+02
5	-2.998825E+02
6	-1.808336E+02
7	-1.017847E+02
8	-2.273584E+01
9	5.631304E+01
10	1.353619E+02
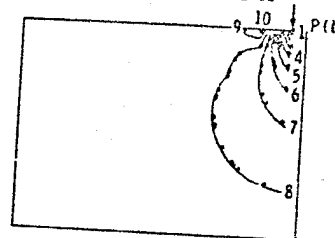
1	7.771991E+02
2	-6.946070E+02
3	-5.920160E+02
4	-4.994229E+02
5	-4.068309E+02
6	-3.142388E+02
7	-2.216468E+02
8	-1.290548E+02
9	-3.646273E+01
10	5.612931E+01

(c) σ_{12} Contours.

(c) σ_{12} Contours.

Figure 8. - Dynamic stress contours in S-glass/epoxy composite flexural specimen after 1 percent contact time.
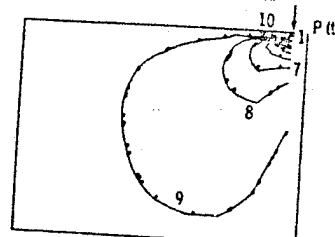
Figure 9. - Dynamic stress contours in Kevlar/epoxy composite flexural specimen after 1 percent of the contact time.

SYMBOL VALUES, psi

1	-2.200180E+03
2	-1.907888E+03
3	-1.615597E+03
4	-1.323305E+03
5	-1.031014E+03
6	-7.387221E+02
7	-4.464305E+02
8	-1.541389E+02
9	1.381526E+02
10	4.304442E+02
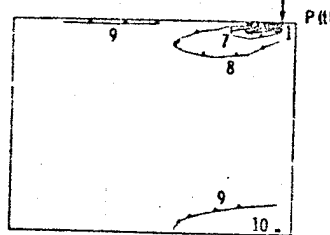
(a) σ_{11} Contours.

1	-1.019117E+03
2	-8.816818E+02
3	-7.442470E+02
4	-6.068122E+02
5	-4.693774E+02
6	-3.319426E+02
7	-1.945078E+02
8	-6.707301E+01
9	8.036180E+01
10	2.177966E+02
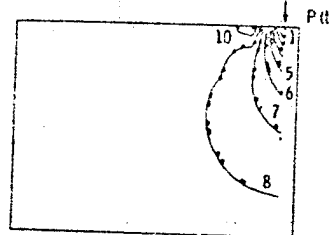
(b) σ_{22} Contours.

1	-7.026985E+02
2	-6.178950E+02
3	-5.830914E+02
4	-4.482878E+02
5	-3.634842E+02
6	-2.786306E+02
7	-1.938771E+02
8	-1.090725E+02
9	-2.426991E+01
10	6.053367E+01
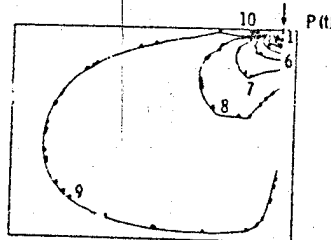
(c) σ_{12} Contours.

Figure 10. – Dynamic stress contours in
T-300/epoxy composite flexural specimen
after 1 percent contact time.
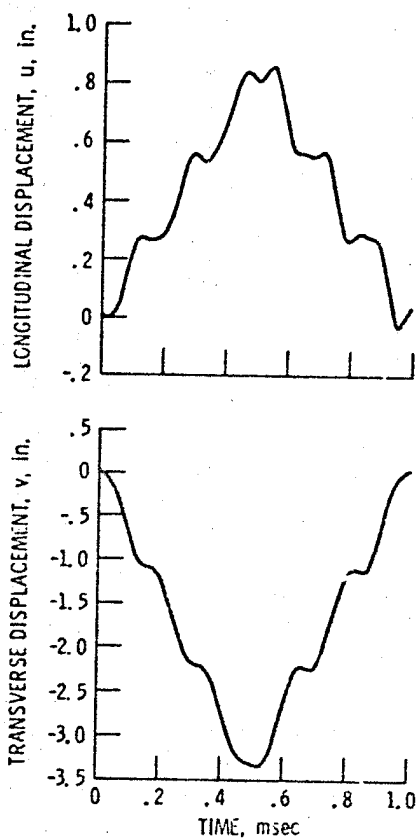
Figure 11. - Displacement response
of point A for S-glass/epoxy
smooth flexural specimen.
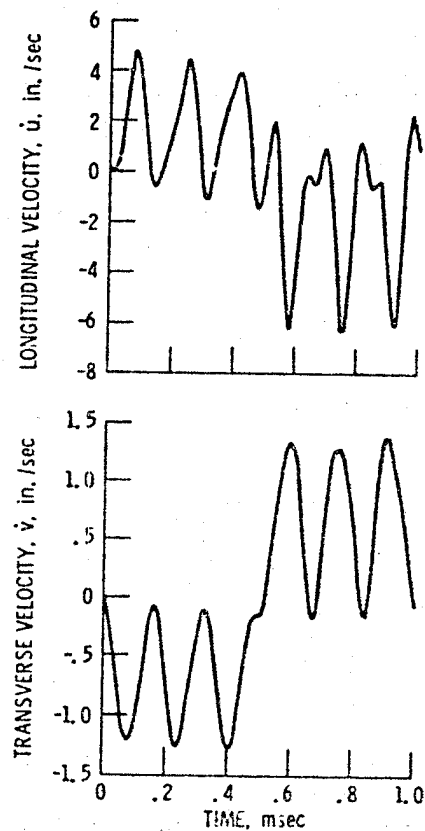
Figure 12. - Velocity response of
point A for S-glass/epoxy smooth
flexural specimen.
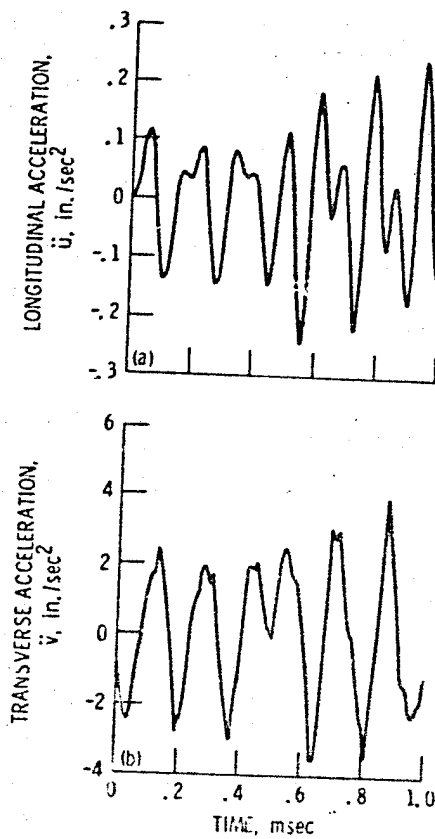
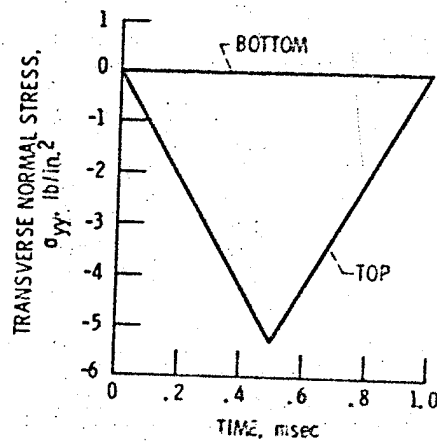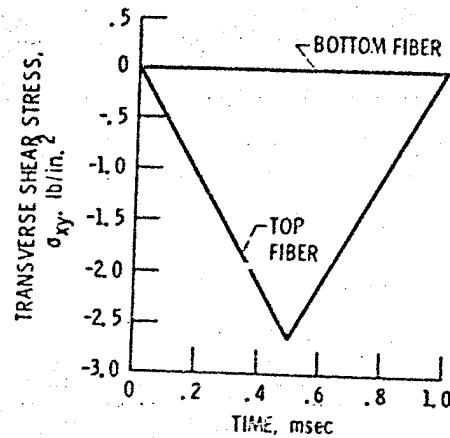Figure 13. – Acceleration response for S-glass/epoxy smooth flexural specimen.
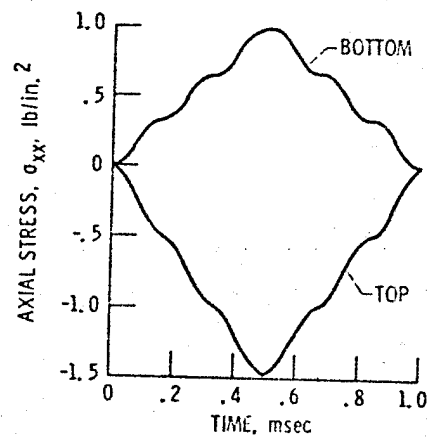
Figure 14. – Axial stress σ_{xx} response of top and bottom elements near points A and B for S-glass/epoxy smooth flexural specimen.
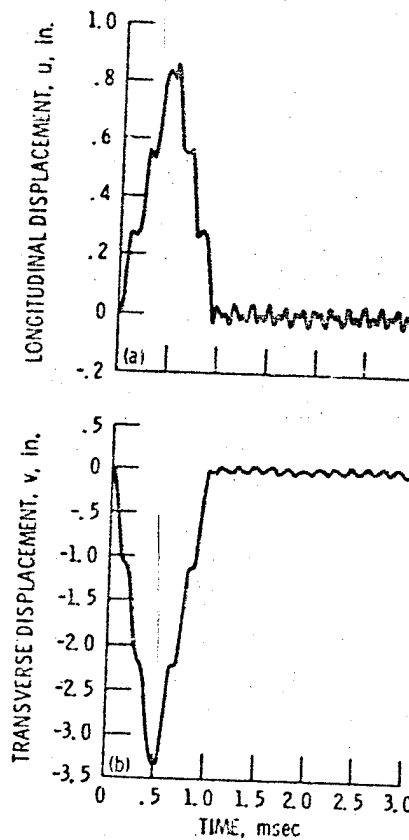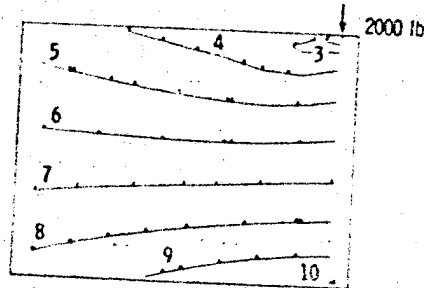
Figure 15. – Transverse normal stress σ_{yy} response of top and bottom elements near points A and B for S-glass/epoxy smooth flexural specimen.

Figure 16. – Transverse shear stress σ_{xy} response of top and bottom elements near points A and B for S-glass/epoxy smooth flexural specimen.

Figure 17. – Displacement response of point A for three contact time periods of S-glass/epoxy smooth flexural specimen.

SYMBOL VALUES, psi

1	-1.494680E+05
2	-1.216115E+05
3	-9.375496E+04
4	-6.589843E+04
5	-3.804191E+04
6	-1.018539E+04
7	1.767114E+04
8	4.552766E+04
9	7.338418E+04
10	1.012407E+05

(a) Static stress contours.

SYMBOL VALUES, psi

1	-5.259623E+04
2	-4.533239E+04
3	-3.806855E+04
4	-3.080471E+04
5	-2.354087E+04
6	-1.627703E+04
7	-9.013191E+03
8	-1.749351E+03
9	5.514490E+03
10	1.277833E+04

(a) Static stress contours.

1	-1.480251E+05
2	-1.205350E+05
3	-9.304484E+04
4	-6.555471E+04
5	-3.806458E+04
6	-1.057445E+04
7	1.691569E+04
8	4.440582E+04
9	7.189595E+04
10	9.938608E+04
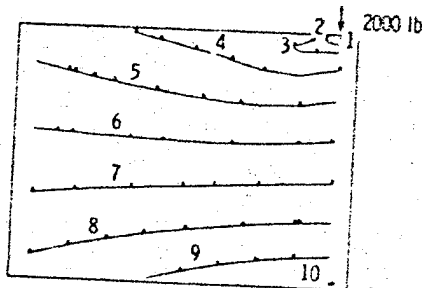
(b) Dynamic stress contours.
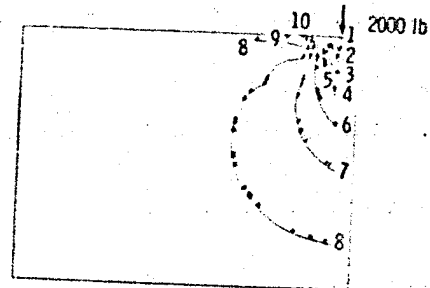
Figure 18. – Comparison of static and dynamic axial stress σ_{xx} contours at peak load for S-glass/epoxy smooth flexural specimens.
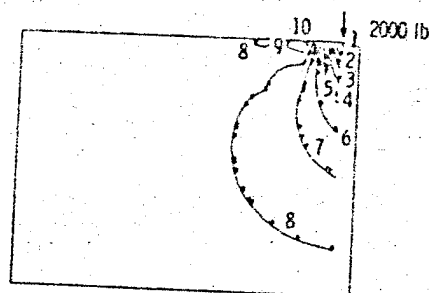
|	
1	-5.248293E+04
2	-4.523803E+04
3	-3.799313E+04
4	-3.074823E+04
5	-2.350333E+04
6	-1.625843E+04
7	-9.013535E+03
8	-1.768636E+03
9	5.476263E+03
10	1.272116E+04

(b) Dynamic stress contours.

Figure 19. – Comparison of static and dynamic transverse normal stress σ_{yy} contours at peak load for S-glass/epoxy smooth flexural specimen.
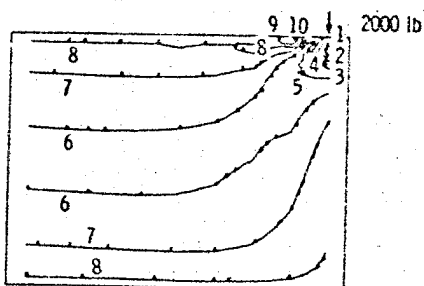
SYMBOL VALUES, psi

1	-2.175306E+04
2	2.182564E+04
3	6.540473E+04
4	1.089836E+05
5	1.525625E+05
6	1.961414E+05
7	2.397203E+05
8	2.832992E+05
9	3.268781E+05
10	3.704570E+05

SYMBOL VALUES, psi

1	-2.867220E+04
2	-2.474687E+04
3	-2.082155E+04
4	-1.689622E+04
5	-1.297089E+04
6	-9.045565E+03
7	-5.129230E+03
8	-1.194911E+03
9	2.730416E+03
10	6.655744E+03

2000 lb

(a) Static stress contours.
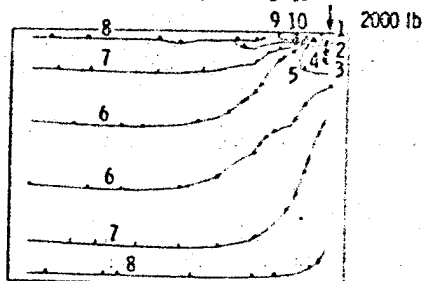
(a) Static stress contours.

1	-2.850863E+04
2	-2.461521E+04
3	-2.072178E+04
4	-1.682836E+04
5	-1.293493E+04
6	-9.041510E+03
7	-5.148086E+03
8	-1.254662E+03
9	2.638762E+03
10	6.532187E+03

1	-2.125020E+04
2	2.137141E+04
3	6.399302E+04
4	1.066146E+05
5	1.492362E+05
6	1.918579E+05
7	2.344795E+05
8	2.771011E+05
9	3.197227E+05
10	3.623443E+05

2000 lb

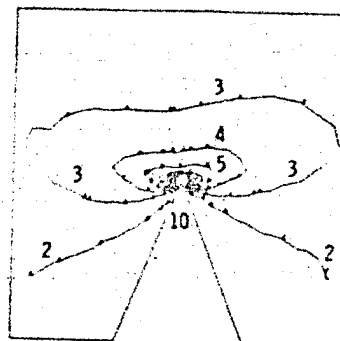(b) Dynamic stress contours.

(b) Dynamic stress contours.

Figure 20. – Comparison of static and dynamic
transverse shear stress σ_{xy} contours at
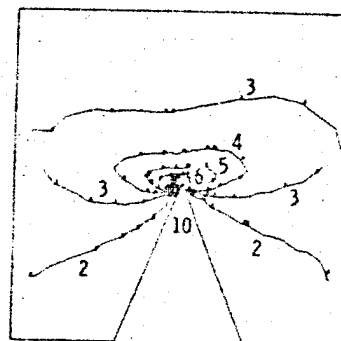peak load for S-glass/epoxy smooth flexural
specimen.
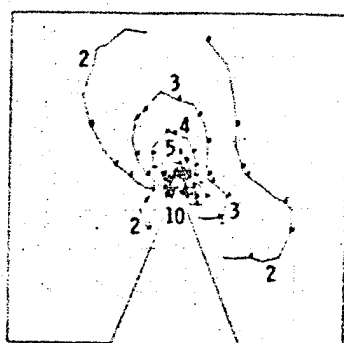
Figure 21. – Comparison of static and
dynamic axial stress σ_{xx} contours
near the notch region at peak load
for S-glass/epoxy notched flexural

SYMBOL VALUES, psi

1	-4.934123E+03
2	9.081599E+03
3	2.309732E+04
4	3.711304E+04
5	5.112877E+04
6	6.514449E+04
7	7.916021E+04
8	9.317593E+04
9	1.071917E+05
10	1.212074E+05

SYMBOL VALUES, psi

1	-9.067550E+04
2	-7.053295E+04
3	-5.039041E+04
4	-3.024786E+04
5	-1.010531E+04
6	1.003724E+04
7	3.017979E+04
8	5.032234E+04
9	7.046488E+04
10	9.060743E+04

(a) Static stress contours.
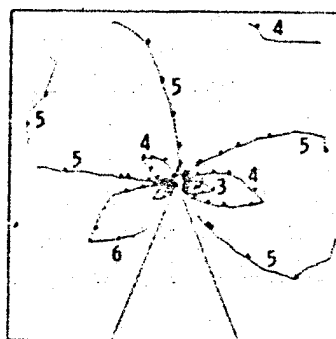
(a) Static stress contours.

1	-4.830871E+03
2	8.877968E+03
3	2.258681E+04
4	3.629565E+04
5	5.000448E+04
6	6.371332E+04
7	7.742216E+04
8	9.113100E+04
9	1.048398E+05
10	1.185487E+05

1	-8.881748E+04
2	-6.911646E+04
3	-4.941543E+04
4	-2.971441E+04
5	-1.001339E+04
6	9.687638E+03
7	2.938866E+04
8	4.908969E+04
9	6.879071E+04
10	8.849173E+04
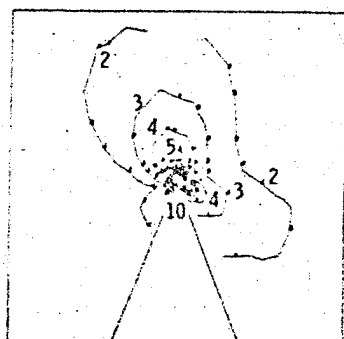
(b) Dynamic stress contours.

Figure 22. – Comparison of static and dynamic transverse normal stress σ_{yy} contours near the notch region at peak load for S-glass/epoxy notched flexural specimen.
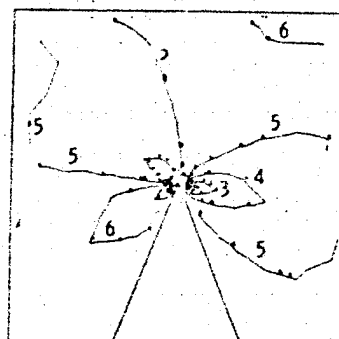
(b) Dynamic stress contours.

Figure 23. – Comparison of static and dynamic transverse shear stress σ_{xy} contours near the notch region at peak load for S-glass/epoxy notched flexural specimen.
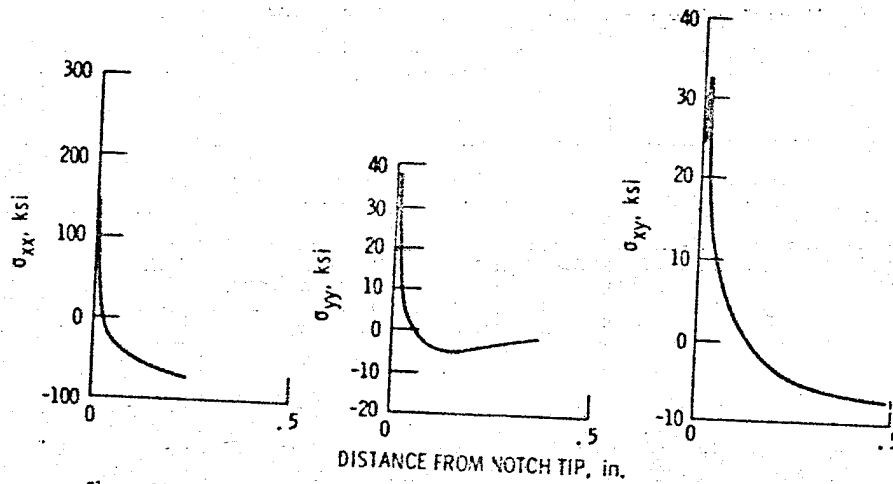
Figure 24. – Stress intensity distribution near the notch tip for S-glass/epoxy notched flexural specimen.

END

DATE

FILMED

AUG 13 1984